

# Composition-induced structural transitions in mixed rare-gas clusters

F. Calvo

*Laboratoire de Physique Quantique, IRSAMC, Université Paul Sabatier,  
118 Route de Narbonne, F31062 Toulouse Cedex, France*

E. Yurtsever

*Koç University, Rumelifeneriyolu, Sariyer, Istanbul 34450, Turkey*

The low-energy structures of mixed Ar–Xe and Kr–Xe Lennard-Jones clusters are investigated using a newly developed parallel Monte Carlo minimization algorithm with specific exchange moves between particles or trajectories. Tests on the 13- and 19- atom clusters show a significant improvement over the conventional basin-hopping method, the average search length being reduced by more than one order of magnitude. The method is applied to the more difficult case of the 38-atom cluster, for which the homogeneous clusters have a truncated octahedral shape. It is found that alloys of dissimilar elements (Ar–Xe) favor polytetrahedral geometries over octahedra due to the reduced strain penalty. Conversely, octahedra are even more stable in Kr–Xe alloys than in Kr<sub>38</sub> or Xe<sub>38</sub>, and they show a core-surface phase separation behavior. These trends are indeed also observed and further analysed on the 55-atom cluster. Finally, we correlate the relative stability of cubic structures in these clusters to the glassforming character of the bulk mixtures.

## I. INTRODUCTION

Clusters of heterogeneous materials show a much richer behavior than their homogeneous counterparts. In many bulk compounds, doping can significantly affect some global property, and alloying is a common way to tailor a completely new kind of material. At the mesoscale level, size is another complicating factor, giving rise to further changes with respect to the macroscopic object. To a large extent, most expectations of nanotechnology have been put into the electronic and catalytic properties of small atomic clusters. Therefore, it should not be surprising that numerous theoretical studies of mixed clusters were devoted to bimetallic clusters. In particular, there has been a significant amount of work at the level of sophisticated electronic structure calculations,<sup>1,2,3</sup> but these were often limited to small sizes due to the numerical effort involved. On a different scale of chemical complexity, many studies have been carried out using explicit, empirical force fields<sup>4,5,6,7,8,9,10,11,12</sup> in order to investigate the segregation properties of these clusters.

There are several driving forces toward mixing or segregation in binary systems:

- (i) the difference in atomic sizes;
- (ii) the difference in surface energies;
- (iii) minimization of the overall strain;
- (iv) the number of interactions between unlike atoms.

These factors can often compete with each other. For instance, minimizing surface energies does usually not increase with the number of interactions between different atoms. Also, even though this is not our prime interest here, it should be noted that kinetic factors can be crucial in this problem.<sup>13</sup>

In particular, Vach and coworkers have found from experiments and simulations of mixed rare-gas clusters that

some anomalous enrichment effects could be observed due to the growth by pick-up of these systems.<sup>14</sup> Very recently, radial segregation and layering have been observed in large Ar/Xe clusters formed in an adiabatic expansion by Tchapyguine *et al.*<sup>15</sup> using photoelectron spectroscopy measurements. These data have also been theoretically interpreted by Amar and Smaby.<sup>16</sup>

Fortunately, mixed rare-gas systems can be quite safely described using simple pairwise potentials such as the Lennard-Jones (LJ) potential. More accurate potentials are of course also available, even though we will have no need for them in the present, mostly methodological work. Hence they are much more convenient to study in a broad size range, not only for their structure but also their dynamics or thermodynamics. It is known from previous studies that the topography of the potential energy surfaces of homogeneous LJ clusters can be very peculiar, as for the sizes 38 or 75.<sup>17</sup> The multiple-funnel structure of these energy landscapes makes it especially hard to locate the most stable structures (global minima) or to simulate the finite-temperature behavior of these clusters in an ergodic way. The effects of mixing different rare-gas atoms on cluster structure and thermodynamics have been studied for the specific size 13 by Frantz on the examples of Ar–Kr mixtures<sup>18</sup> as well as Ne–Ar mixtures.<sup>19</sup> Fanourgakis *et al.* have also investigated these latter compounds.<sup>20</sup> A systematic work of Ar–Xe mixed clusters of 13 and 19 atoms has been carried out by Munro and coworkers,<sup>21</sup> including some global optimization and Monte Carlo simulations. Mixed clusters involving lighter species such as H<sub>2</sub> and D<sub>2</sub> have been investigated using path-integral Monte Carlo simulations (PIMC) by Chakravarty.<sup>22</sup> More recently, Sabo, Doll and Freeman reported a rather complete study of the energy landscapes<sup>23,24</sup> and melting phase change<sup>25</sup> in mixed Ar–Ne clusters. In this work quantum delocalization and the effects of impurities on cluster properties were also accounted for using PIMC techniques.

The main conclusion of these studies is that atomic heterogeneity can be responsible for a drastic increase in complexity of the energy landscapes of rare-gas clusters. This complexity is manifested by numerous new low-lying minima in competitive funnels, characterized by the same overall geometrical arrangement but different permutations of unlike atoms. Following Jellinek and Krissinel,<sup>4</sup> we will refer to such isomers as “homotops.” The presence of several homotops on a given energy landscape often induces solid-solid transitions, which can be detected by some feature in the heat capacity,<sup>18,19,20,21,26</sup> even though they can be washed out by quantum effects.<sup>25</sup> As shown by Munro *et al.*,<sup>21</sup> the various funnels corresponding to different homotops of a same geometry are separated by significant energy barriers. This explains the difficulty or even failure of simulation methods to achieve ergodic sampling of these systems, albeit small.<sup>21</sup> A similar situation is found in Lennard-Jones polymers,<sup>27</sup> where a large number of isomers are based on the same geometrical arrangement, differing only in the path linking the monomers.

Beyond the actual rare-gases, binary Lennard-Jones compounds have been investigated in both the cluster and bulk regimes. Clarke and coworkers looked at phase separation of small particles with equal compositions.<sup>28</sup> Based on Monte Carlo simulations, they sketched a phase diagram in the general structure of liquid clusters. Bulk binary Lennard-Jones systems have been seen to provide relatively simple numerical models for glass formation.<sup>29,30,31,32,33,34</sup> Most often, the LJ interactions in such studies have been tuned in a non-additive way in order to hinder crystallisation. In another related work, Lee and coworkers<sup>35</sup> have investigated the role of atomic size ratio in binary and ternary metallic alloys.

Interestingly, several links between the physics and chemistry of clusters and those of supercooled liquids and glasses have been established since the pioneering work by Frank.<sup>36</sup> The initial suggestion that the local order in simple liquids is not crystalline but icosahedral<sup>36</sup> (more generally polytetrahedral) has since been verified experimentally<sup>37</sup> and theoretically.<sup>29,38</sup> From the clusters viewpoint, the favored finite-size structures of good model glassformers have been shown by Doye and coworkers to be polytetrahedral.<sup>39</sup>

The 38-atom homogeneous Lennard-Jones cluster is known to show some glassy properties, especially slow relaxation to the ground state,<sup>40</sup> due to the competition between two stable funnels on the energy landscape, corresponding to truncated octahedral and icosahedral shapes, respectively. Due to entropic effects,<sup>40,41</sup> a solid-solid transition occurs between the two funnels, at temperatures lower than the melting point. The crystal-like configuration of this cluster makes it a good candidate to further investigate the relationship between cluster structure and criteria for glassification.

Because homogeneous LJ<sub>38</sub> constitutes a relatively difficult task for global optimization algorithms, binary clusters of the same size can be expected to be much

worse. In this paper, we propose a simple but efficient way to deal with the multiple new minima introduced by unlike atoms within a general Monte Carlo global minimization scheme. This algorithm will then be applied to the 38- and 55-atom cases, in mixtures of Xe with either Ar or Kr atoms. In the next section, we present the method and test it on the simple cases of the 13- and 19-atom clusters. In Sec. III we give our results obtained at sizes 38 and 55 and we correlate them to the different glassforming abilities of the bulk mixtures. We finally conclude in Sec. IV.

## II. METHODS

Global optimization of cluster structure<sup>42</sup> is currently best achieved using either genetic algorithms<sup>43</sup> or the Monte Carlo+minimization method,<sup>44</sup> also known as basin-hopping (BH).<sup>45</sup> The case of homogeneous Lennard-Jones clusters is among the most documented of cluster physics, and an up-to-date table of putative global minima can be found in Ref. 46. Even though it can never be guaranteed that global minimization has been successful, it is likely that all important structural forms of LJ clusters have been found up to more than 100 atoms. These include icosahedral, truncated octahedral, decahedral as well as tetrahedral arrangements.

Compared to homogeneous clusters, the available data on heterogeneous systems is rather scarce. Besides the specific works by Frantz on the 13-atom Ne-Ar and Kr-Ar clusters,<sup>18,19</sup> Munro *et al.* used a parallel version of the BH scheme, similar to the replica-exchange Monte Carlo method,<sup>47</sup> where several trajectories are run simultaneously at various temperatures.<sup>21</sup> Although these authors looked at moderately large clusters, they reported significant difficulties to locate global minima at specific compositions, as in Xe<sub>10</sub>Ar<sub>3</sub> or Xe<sub>13</sub>Ar<sub>6</sub>, for instance.<sup>21</sup>

### A. Optimization algorithm

A natural problem occurring using the basin-hopping method is that many of the low-lying minima are expected to be related to each other via particle exchange. Such a process only occurs via large deformations of the remaining cluster, hence it is quite improbable. As in condensed matter physics,<sup>48,49,50</sup> allowing exchange moves between particles as a possible Monte Carlo step may result in notably faster convergence, provided that the interactions are not too dissimilar. Actually, optimization of mixed clusters on the lattice formed by the homogeneous system has already been studied by Robertson and coworkers.<sup>51</sup> Here we do not wish to restrict to such situations.

In the framework of global optimization methods, the local minimization stage removes the possible energetic penalty associated to replacing a small atom by a bigger one. We can thus expect some increased efficiency

of the algorithm in case of multiple homotops. Now we convert the extra numerical cost of running parallel trajectories at various temperatures into running them at various compositions, at the same fixed temperature  $T$  for all compositions. For a  $X_pY_{n-p}$  compound, each of the  $n$  trajectories is then labelled with the number  $p$  of X atoms, running from 0 to  $n$ . Exchange moves between adjacent trajectories (from  $p$  to  $p+1$ ) thus need to incorporate the transmutation of two atoms (one for each configuration) into the other atom type to preserve composition. As in most Monte Carlo processes, the probability of attempting such moves must be set in advance as a parameter.

The global optimization algorithm can thus be summarized into its main steps. Keeping the above notations for atom types, and denoting  $\mathbf{R}_i^{(p)}$  the configuration at step  $i$  of trajectory  $p$ , we start the optimization process using fully random configurations, but locally optimized.

1. With probability  $P_{\text{ex}}$ , it is decided whether an exchange between adjacent trajectories will be attempted or not. If so, then the two trajectories involved in the exchange are determined randomly.
2. For each composition  $p$  not concerned by any exchange, a new configuration  $\mathbf{R}_{i+1}^{(p)}$  is generated from  $\mathbf{R}_i^{(p)}$  using either several particle exchanges or large atomic moves. The probability to select particle exchanges is denoted  $P_{\text{swap}}$ , and the number of simultaneous exchanges is allowed to fluctuate randomly between 1 and  $N_{\text{swap}}^{\text{max}}$ . If atomic moves are selected, then each atom is displaced randomly around its previous location in the three directions by a random amount of maximum magnitude  $h^{(p)}$ . In both cases,  $\mathbf{R}_{i+1}^{(p)}$  is obtained after local minimization.
3. In case of an exchange between adjacent trajectories, the two configurations  $\mathbf{R}_i^{(p)}$  and  $\mathbf{R}_i^{(p+1)}$  corresponding to these trajectories are then swapped, one X atom of  $\mathbf{R}_i^{(p)}$  being transmuted into Y, and one Y atom of  $\mathbf{R}_i^{(p+1)}$  being transmuted into X. Again, the configurations  $\mathbf{R}_{i+1}^{(p)}$  and  $\mathbf{R}_{i+1}^{(p+1)}$  are obtained after local minimization.
4. Each new configuration is accepted with the usual Metropolis acceptance probability at temperature  $T$ .

The algorithm has two main parameters, namely  $P_{\text{ex}}$  and  $P_{\text{swap}}$ . The maximum number of particle exchange moves,  $N_{\text{swap}}^{\text{max}}$ , was set to 4 in this study. We expect that better results could be obtained by adjusting this parameter appropriately, probably taking higher values for larger clusters or for compositions close to 50%. The amplitude of atomic displacement,  $h^{(p)}$ , is set to half the equilibrium distance in the  $X_2$  dimer for  $p=0$ , half the equilibrium distance in the  $Y_2$  dimer for  $p=n$ , and is interpolated linearly between these two values for  $0 <$

$p < n$ . In the present work, the exchange probabilities were taken as  $P_{\text{ex}} = 0.5$  and  $P_{\text{swap}} = 0.9$ , hence allowing a rather large probability of sampling among homotops of a same structure.

## B. Benchmark calculations

Low-energy structures for mixtures of xenon with either argon or krypton atoms have been first investigated for the sizes  $n=13$  and  $n=19$ , as there are quantitative global optimization data available for Ar–Xe clusters from the Jordan group.<sup>21</sup> We have adjusted the LJ values used by Leitner *et al.*<sup>52</sup> to reproduce the clusters energies found by Munro and coworkers.<sup>21</sup> With respect to argon, the present data for  $\sigma$  and  $\varepsilon$  are thus  $\sigma_{\text{KrKr}} = 1.12403$ ,  $\sigma_{\text{XeXe}} = 1.206$ ,  $\sigma_{\text{KrXe}} = 1.16397$ ,  $\sigma_{\text{ArXe}} = 1.074$ ,  $\varepsilon_{\text{KrKr}} = 1.373534$ ,  $\varepsilon_{\text{XeXe}} = 1.852$ ,  $\varepsilon_{\text{KrXe}} = 1.59914$ , and  $\varepsilon_{\text{ArXe}} = 1.48$ . Global optimization of Ar–Xe and Kr–Xe clusters was performed using the parallel algorithm previously described, simultaneously for all compositions, for a maximum number of 10000 minimization steps per trajectory, and at  $T=0$ . Ten independent runs were carried out to estimate an average search length for each composition. All global minima reported by Munro *et al.* were always found within the number of MC steps allowed.

The results for  $\text{Ar}_n\text{Xe}_{13-n}$  and  $\text{Kr}_n\text{Xe}_{13-n}$  clusters are given in Table I. The average search length is generally higher for compositions close to 50%, for which the number of homotops is maximum for a given isomer, regardless of symmetry. The statistics presently obtained for Ar–Xe clusters show that the average search is between 10 and 1000 times faster than using conventional parallel basin-hopping.<sup>21</sup> Kr–Xe clusters roughly exhibit the same level of difficulty, but we do not see any strong evidence for particularly severe cases:  $\text{Ar}_3\text{Xe}_{10}$  even seems to be one of the easiest.

Similarly, the results obtained for  $\text{Ar}_n\text{Xe}_{19-n}$  clusters show a significant improvement over fixed-composition basin-hopping.<sup>21</sup> They are given in Table II along with the corresponding data for  $\text{Kr}_n\text{Xe}_{19-n}$  clusters. This time, the algorithm is about 1–100 times faster depending on  $n$ , the average search length being still longer for equal compositions. For both the 13- and 19-atom clusters, all global minima are homotops of either the single or double icosahedron. This situation is particularly suited for our algorithm, especially the exchange moves.

Initially, the configurations at all compositions are random. The chances to locate the proper structure (without any consideration of the homotops) increase linearly with the number of trajectories. As soon as the right structure is found, the algorithm naturally optimizes atom types to find the most stable homotop, hence the global minimum. But it can also communicate the structure to the adjacent trajectories, until all compositions only need to sample among the permutational homotops.

When the interactions are not too dissimilar (as in Kr–

TABLE I: Global optimization results for  $\text{Ar}_n\text{Xe}_{13-n}$  and  $\text{Kr}_n\text{Xe}_{13-n}$  clusters. The search length is the average over 10 independent runs of the number of Monte Carlo steps needed to find the global minimum. Energies are given in LJ units for argon.

$\text{Ar}_n\text{Xe}_{13-n}$ cluster	Global minimum energy	Average search length	$\text{Kr}_n\text{Xe}_{13-n}$ cluster	Global minimum energy	Average search length
$\text{Xe}_{13}$	-82.093	3.2	$\text{Xe}_{13}$	-82.093	3.0
$\text{ArXe}_{12}$	-78.698	7.9	$\text{KrXe}_{12}$	-81.014	9.6
$\text{Ar}_2\text{Xe}_{11}$	-76.274	9.6	$\text{Kr}_2\text{Xe}_{11}$	-79.263	4.3
$\text{Ar}_3\text{Xe}_{10}$	-74.015	5.8	$\text{Kr}_3\text{Xe}_{10}$	-77.550	5.7
$\text{Ar}_4\text{Xe}_9$	-71.597	8.6	$\text{Kr}_4\text{Xe}_9$	-75.869	26.1
$\text{Ar}_5\text{Xe}_8$	-69.017	14.0	$\text{Kr}_5\text{Xe}_8$	-74.186	25.8
$\text{Ar}_6\text{Xe}_7$	-66.584	37.2	$\text{Kr}_6\text{Xe}_7$	-72.498	26.4
$\text{Ar}_7\text{Xe}_6$	-63.791	19.4	$\text{Kr}_7\text{Xe}_6$	-70.844	45.2
$\text{Ar}_8\text{Xe}_5$	-60.733	13.9	$\text{Kr}_8\text{Xe}_5$	-69.141	18.3
$\text{Ar}_9\text{Xe}_4$	-57.851	22.7	$\text{Kr}_9\text{Xe}_4$	-67.473	4.7
$\text{Ar}_{10}\text{Xe}_3$	-54.594	12.0	$\text{Kr}_{10}\text{Xe}_3$	-65.802	11.5
$\text{Ar}_{11}\text{Xe}_2$	-51.122	7.5	$\text{Kr}_{11}\text{Xe}_2$	-64.128	4.1
$\text{Ar}_{12}\text{Xe}$	-47.698	4.1	$\text{Kr}_{12}\text{Xe}$	-62.490	2.4
$\text{Ar}_{13}$	-44.327	2.7	$\text{Kr}_{13}$	-60.884	2.3

TABLE II: Global optimization results for  $\text{Ar}_n\text{Xe}_{19-n}$  and  $\text{Kr}_n\text{Xe}_{19-n}$  clusters. The search length is the average over 10 independent runs of the number of Monte Carlo steps needed to find the global minimum. Energies are given in LJ units for argon.

$\text{Ar}_n\text{Xe}_{19-n}$ cluster	Global minimum energy	Average search length	$\text{Kr}_n\text{Xe}_{19-n}$ cluster	Global minimum energy	Average search length
$\text{Xe}_{19}$	-134.566	72.4	$\text{Xe}_{19}$	-134.566	70.7
$\text{ArXe}_{18}$	-131.819	64.3	$\text{KrXe}_{18}$	-133.651	94.0
$\text{Ar}_2\text{Xe}_{17}$	-129.116	80.3	$\text{Kr}_2\text{Xe}_{17}$	-132.701	109.8
$\text{Ar}_3\text{Xe}_{16}$	-126.547	85.2	$\text{Kr}_3\text{Xe}_{16}$	-130.088	84.3
$\text{Ar}_4\text{Xe}_{15}$	-123.764	238.2	$\text{Kr}_4\text{Xe}_{15}$	-129.067	167.2
$\text{Ar}_5\text{Xe}_{14}$	-120.786	196.6	$\text{Kr}_5\text{Xe}_{14}$	-127.284	175.4
$\text{Ar}_6\text{Xe}_{13}$	-118.284	221.2	$\text{Kr}_6\text{Xe}_{13}$	-125.498	265.9
$\text{Ar}_7\text{Xe}_{12}$	-115.681	391.8	$\text{Kr}_7\text{Xe}_{12}$	-123.709	334.6
$\text{Ar}_8\text{Xe}_{11}$	-113.075	387.9	$\text{Kr}_8\text{Xe}_{11}$	-121.951	319.5
$\text{Ar}_9\text{Xe}_{10}$	-110.242	264.2	$\text{Kr}_9\text{Xe}_{10}$	-120.115	287.1
$\text{Ar}_{10}\text{Xe}_9$	-107.531	295.8	$\text{Kr}_{10}\text{Xe}_9$	-118.304	243.6
$\text{Ar}_{11}\text{Xe}_8$	-104.576	193.8	$\text{Kr}_{11}\text{Xe}_8$	-116.521	187.4
$\text{Ar}_{12}\text{Xe}_7$	-101.811	235.5	$\text{Kr}_{12}\text{Xe}_7$	-114.736	214.3
$\text{Ar}_{13}\text{Xe}_6$	-98.110	158.5	$\text{Kr}_{13}\text{Xe}_6$	-112.947	201.3
$\text{Ar}_{14}\text{Xe}_5$	-94.396	247.3	$\text{Kr}_{14}\text{Xe}_5$	-111.189	188.8
$\text{Ar}_{15}\text{Xe}_4$	-90.438	121.3	$\text{Kr}_{15}\text{Xe}_4$	-108.863	176.5
$\text{Ar}_{16}\text{Xe}_3$	-86.328	131.2	$\text{Kr}_{16}\text{Xe}_3$	-106.609	115.1
$\text{Ar}_{17}\text{Xe}_2$	-81.907	97.3	$\text{Kr}_{17}\text{Xe}_2$	-104.332	10.2
$\text{Ar}_{18}\text{Xe}$	-77.298	86.8	$\text{Kr}_{18}\text{Xe}$	-102.036	98.1
$\text{Ar}_{19}$	-72.660	62.2	$\text{Kr}_{19}$	-99.801	69.8

Xe clusters), it is likely that the mixed clusters share the same isomer as the global minimum of the homogeneous cluster, which justifies the lattice approach of Robertson *et al.*<sup>51</sup> The problem is then reduced to locating the most stable homotops. By setting  $P_{\text{swap}}$  to one and starting

all trajectories from this minimum, the algorithm can be even more successful, and we estimated the average search length to be further reduced by a factor about 3 with respect to the values given in Table II. However, when the interactions differ significantly among atoms

types, or when the energy landscape of the homogeneous cluster does not display a single steep funnel, it becomes much harder to make a guess about structure in these binary clusters.

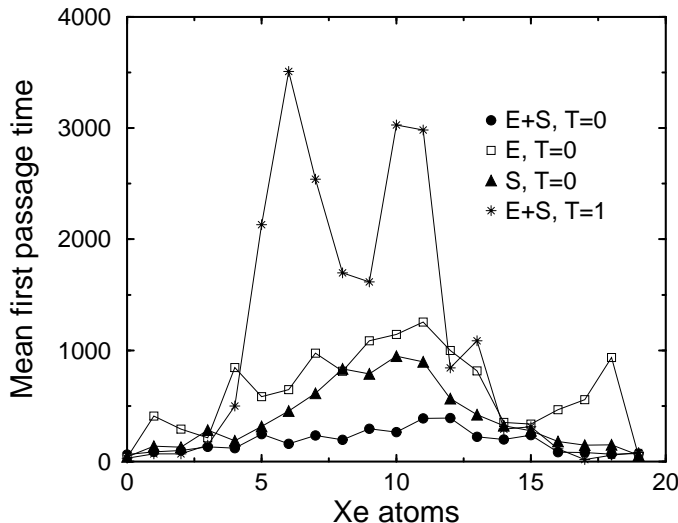


FIG. 1: Mean first passage time of the parallel optimization algorithm to locate the global minimum structure of  $\text{Ar}_{19-n}\text{Xe}_n$  clusters versus  $n$ . The average is performed over 10 independent runs. The results are shown at zero temperature, with or without exchange moves (E) between trajectories, with or without swap moves between atom types (S). The results at  $T = 1$  with both kinds of moves are also displayed.

Fig. 1 shows the mean first passage time needed to locate the global minima of  $\text{Ar}_{19-n}\text{Xe}_n$  using the algorithm under different conditions. Disabling swap moves between atom types or exchange moves between adjacent trajectories usually attenuates the efficiency. Employing a rather high temperature is even worse, because the cluster may easily leave its optimal lattice. This contrasts with optimizing homogeneous clusters, where using a nonzero temperature helps the system to escape from a funnel.<sup>53</sup> However, if the energy gap between homotops of the same lattice increases and gets close to the gap between different lattices, we expect the zero temperature method not to be the best. But in such cases, even the notion of a lattice should be questioned.

### III. STRUCTURAL TRANSITIONS

In this section we focus on two larger sizes, for which no global optimization result is available. The  $\text{LJ}_{38}$  cluster is characterized by its archetypal two-funnel energy landscape.<sup>40</sup> The high free-energy barrier separating these two funnels and the higher entropy of the less stable minima of the icosahedral funnel make it particularly hard to locate the truncated octahedral lowest-energy minimum using unbiased global optimization algorithms.

Hence it is not surprising that this peculiar structure was first found by construction.<sup>56,57</sup>

#### A. Composition-induced transitions in the 38-atom clusters

We have attempted to locate global minima for binary Ar–Xe and Kr–Xe clusters of size 38, using the parallel basin-hopping algorithm previously described. Because of the huge number of homotops at this size, and most importantly because of the structural competition between icosahedra and truncated octahedra, we cannot be fully confident that the global optimization was successful. Therefore, the energies reported in Table III for Ar–Xe clusters should be taken with caution, as they could probably be bettered. The same data for 38-atom Kr–Xe clusters is also reported in Table V.

Specifically to this cluster size, all minima found during the optimization process were categorized as either icosahedral or cubic-like, depending on the energy of the corresponding homogeneous isomer found by quenching. In cases where the cubic isomer was not found among the isomers, we performed additional optimizations starting from this structure, setting  $P_{\text{swap}}$  to one. This mainly occurred for Ar–Xe clusters. Eventually, two series of minima were obtained for each of the icosahedral and octahedral funnels. We did not find any decahedral isomer that could compete with these structural types, even though some evidence for stabilizing decahedra by doping was reported in Ref. 58.

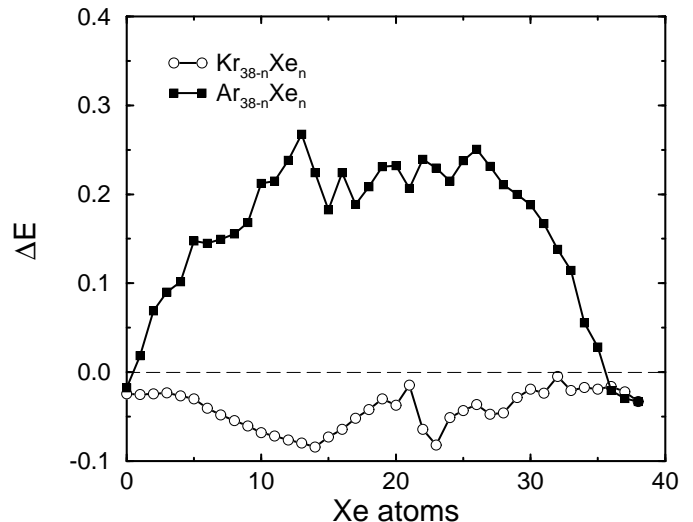


FIG. 2: Energy difference  $\Delta E = E_{\text{fcc}} - E_{\text{ico}}$  between the most stable cubic and icosahedral isomers of  $\text{Kr}_{38-n}\text{Xe}_n$  (empty circles) and  $\text{Ar}_{38-n}\text{Xe}_n$  (full squares).  $\Delta E$  is given in reduced Lennard-Jones unit of Argon (approximately 120 K).

We have represented in Fig. 2 the relative energy differences  $\Delta E = E_{\text{fcc}} - E_{\text{ico}}$  between the most stable cubic

TABLE III: Global optimization results for  $\text{Ar}_{38-n}\text{Xe}_n$ . The energies are given in LJ units for argon, and the symmetry and mixing ratios defined by Eq. (1) are reported.

$n$	Mixing ratio	Energy	Point group	$n$	Mixing ratio	Energy	Point group
0	0	-173.928	$O_h$	20	0.58	-268.683	$C_1$
1	0.03	-179.232	$C_s$	21	0.59	-272.465	$C_1$
2	0.06	-186.333	$C_s$	22	0.56	-276.924	$C_s$
3	0.15	-191.890	$C_1$	23	0.61	-280.169	$C_s$
4	0.19	-197.767	$C_1$	24	0.60	-283.955	$C_{2v}$
5	0.22	-203.421	$C_s$	25	0.60	-287.679	$C_s$
6	0.25	-208.709	$C_s$	26	0.59	-290.973	$C_1$
7	0.28	-213.815	$C_1$	27	0.58	-294.157	$C_s$
8	0.32	-218.631	$C_s$	28	0.58	-297.320	$C_{2v}$
9	0.34	-223.491	$C_1$	29	0.56	-300.202	$C_{2v}$
10	0.36	-228.209	$C_1$	30	0.50	-303.484	$C_1$
11	0.39	-232.771	$C_1$	31	0.51	-305.987	$C_1$
12	0.40	-237.337	$C_1$	32	0.46	-308.404	$C_1$
13	0.43	-241.887	$C_s$	33	0.43	-310.521	$C_1$
14	0.44	-246.117	$C_1$	34	0.38	-311.708	$C_1$
15	0.45	-249.677	$C_s$	35	0.31	-313.772	$C_1$
16	0.46	-253.593	$C_s$	36	0.25	-315.988	$C_1$
17	0.46	-257.184	$C_s$	37	0.14	-318.860	$C_1$
18	0.46	-261.079	$C_s$	38	0	-322.115	$O_h$
19	0.56	-264.927	$C_1$				

isomers and the most stable icosahedral isomers, as they were obtained from our optimization scheme, for both the Ar–Xe and Kr–Xe mixtures. Besides some strong variations sometimes seen from one composition to the next, and which can be attributed to usual finite-size effects, general trends can be clearly observed.

First,  $\text{Kr}_{38-n}\text{Xe}_n$  clusters are always most stable in the cubic shape. Actually, changing the composition most often further stabilizes truncated octahedra, and only rarely enhances the stability of icosahedra, which occurs for  $n > 29$  and  $n = 21$ . Conversely  $\text{Ar}_{38-n}\text{Xe}_n$  clusters are preferentially found icosahedral, exceptions being  $n > 35$  and  $n = 0$ . This is an example of a composition-induced structural transition between the two funnels of the energy landscape.

From a computational point of view, it should be noted that the optimization algorithm was able to locate the truncated octahedral minima for Kr–Xe clusters by itself, starting from disordered minima, and that the extra runs starting from this structure only produced slightly more stable homotops. This is another illustration of the efficiency of the present parallel optimization method.

The general degree of disorder is higher in icosahedral structures than in the cubic-like isomer. Hence it is more difficult to put up the latter geometry with very unlike interactions, as in Ar–Xe clusters. Cubic homotops of argon with xenon are rather distorted, but the strain is much lower with krypton instead of argon. Examples of global minima obtained at compositions  $n = 9, 19,$  and  $29$  are represented in Fig. 3. In Kr–Xe compounds, a

progressive core-surface phase separation is seen with Kr atoms outside, in agreement with energetic arguments: atoms with the larger  $\varepsilon$  prefer to occupy interior sites. In icosahedral clusters, the strain increases at such sites, especially in polytetrahedral systems. Icosahedral Kr–Xe clusters also prefer to have Xe atoms at the center, but the increased strain is too high a penalty, which explains that cubic structures are favored over icosahedra.

In general, no complete phase separation is found in Ar–Xe clusters, even though Ar atoms seem to fit best at the centre of the cluster. In both cases, surface energies thus play an important role. Mixing in these clusters can be estimated using radial distribution functions.<sup>54</sup> Here we use the same index as Jellinek and Krissinel,<sup>4</sup> namely the overall mixing ratio  $\gamma$  defined as<sup>4</sup>

$$\gamma(X_p Y_{n-p}) = \frac{E_{X_p Y_{n-p}} - E_{X_p}(X_p X_{n-p}) - E_{Y_{n-p}}(Y_p Y_{n-p})}{E_{X_p Y_{n-p}}}, \quad (1)$$

where  $E_{X_p Y_{n-p}}$  is the binding energy of cluster  $X_p Y_{n-p}$ ,  $E_{X_p}(X_p X_{n-p})$  the binding energy of subcluster  $X_p$  in the homogeneous cluster  $X_p X_{n-p}$  at the same atomic configuration as  $X_p Y_{n-p}$ , and a similar definition for the last term of Eq. (1). As seen from Table III, the mixing ratio increases notably in Ar–Xe clusters, up to more than 60% for some compositions. Kr–Xe clusters, despite exhibiting some core-surface segregation, show similar variations of the mixing ratio with composition, with only slightly smaller values of  $\gamma$ . Therefore the mixing ratio, as de-

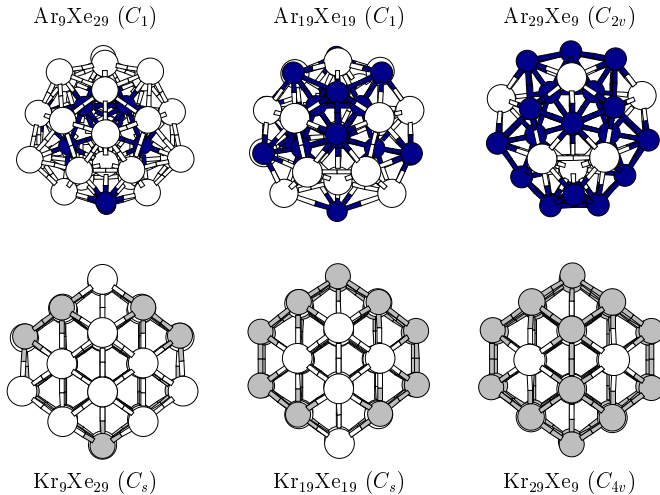


FIG. 3: Putative global minima found for several  $\text{Ar}_{38-n}\text{Xe}_n$  and  $\text{Kr}_{38-n}\text{Xe}_n$  clusters. Argon, krypton, and xenon atoms are represented as black, gray, and white balls, respectively. The point groups are indicated.

fined in Eq. (1), is a rather ambiguous parameter for quantifying the extent of mixing in this small cluster.

The optimal structure of an homogeneous cluster described with a pairwise potential results from a competition between maximizing the number of nearest neighbors and minimizing the strain energy, or penalty induced by distorting these bonds.<sup>57</sup> Binary Lennard-Jones systems exhibit several extra complications due to the various ways of rearranging atom types in a given structure. In these systems, the strain varies notably among the homotops, especially in clusters made of very unlike atoms. However, our results indicate that the same general rules hold for homogeneous and heterogeneous systems. In  $\text{Ar}_{19}\text{Xe}_{19}$ , the strain is rather high, but the number of contacts is also high. In  $\text{Kr}_{19}\text{Xe}_{19}$ , both the strain and the number of nearest neighbors are much smaller.

To investigate the role of heterogeneity on the strain, we have computed the various contributions to the reduced strain energies in  $\text{Ar}_{38-n}\text{Xe}_n$  clusters. The strain energies are defined for Ar–Ar, Xe–Xe, and Ar–Xe interactions as follows:<sup>57</sup>

$$\begin{aligned} E_{\text{Ar–Ar}}^{\text{strain}} &= V_{\text{Ar–Ar}}^{\text{LJ}} + N_{\text{Ar–Ar}}^{\text{nn}} \varepsilon_{\text{Ar–Ar}}, \\ E_{\text{Ar–Xe}}^{\text{strain}} &= V_{\text{Ar–Xe}}^{\text{LJ}} + N_{\text{Ar–Xe}}^{\text{nn}} \varepsilon_{\text{ArXe}}, \\ E_{\text{Xe–Xe}}^{\text{strain}} &= V_{\text{Xe–Xe}}^{\text{LJ}} + N_{\text{Xe–Xe}}^{\text{nn}} \varepsilon_{\text{Xe–Xe}}. \end{aligned}$$

In these equations,  $V_{X–Y}^{\text{LJ}}$  is the (negative) total binding energy between atoms  $X$  and  $Y$ ,  $N_{X–Y}^{\text{nn}}$  is the number of  $X–Y$  nearest neighbors, and  $\varepsilon_{X–Y}$  is the Lennard-Jones well depth corresponding to the interaction between  $X$  and  $Y$  atoms. Reduced strain energies are then defined as  $e^{\text{strain}} = E^{\text{strain}}/N^{\text{nn}}\varepsilon$ , in order to account for the different magnitudes of the interactions among atom

types. According to these definitions, the strain energies are always positive quantities. The strain energies in  $\text{Ar}_{38-n}\text{Xe}_n$  clusters are represented versus composition in Fig. 4. They give us some insight about the possible ways of reducing strain.

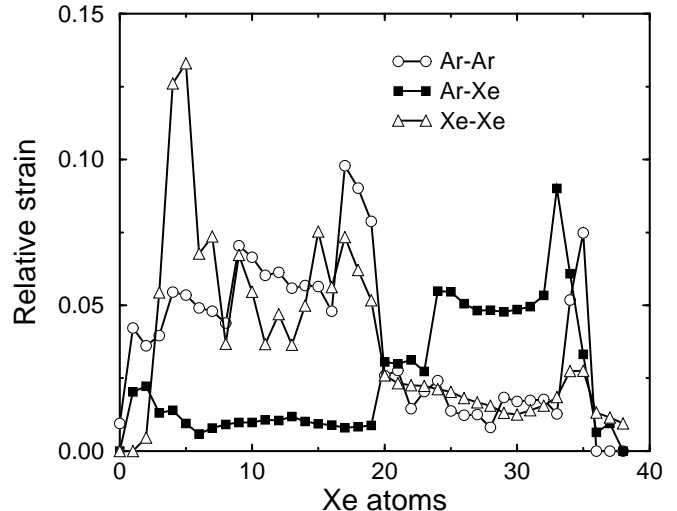


FIG. 4: Reduced strain energies for alike and unlike interactions in  $\text{Ar}_{38-n}\text{Xe}_n$  clusters, versus composition  $n$ .

The pattern exhibited by the reduced strain versus composition shows different behaviors for clusters having mostly argon or xenon atoms. For  $n < 20$ , most strain is carried by interactions between alike atoms. This case is illustrated by  $\text{Ar}_9\text{Xe}_{29}$  in Fig. 3, where a kind of core/surface phase separation occurs. Here surface energies are also important, but the situation is rather different from mixed cubic Kr–Xe clusters. Because having the xenon atoms at the inner sites of the icosahedral structure would maximise the strain of these atoms, it is much more favorable to have the smaller atoms inside and the xenon atoms outside. The cubic Kr–Xe structures, on the other hand, are not especially strained, and having the smaller atoms inside would lead to an energetic penalty.

When the number of Ar atoms increases above about 19 in the 38-atom cluster, interactions between unlike atoms are significantly more strained. The case of  $\text{Ar}_{29}\text{Xe}_9$  depicted in Fig. 3 is particularly informative: Xe atoms are located scarcely among the icosahedral cluster, and relieve the structure from too much strain at the expense of only few Xe–Xe interactions. In this case, cluster structure is driven by the number of unlike interactions.

It is also worth noting that a few compositions are especially weakly strained; this occurs when the global minimum is octahedral, but also in the range  $19 < n < 24$ . For these latter clusters, the core/surface segregation and the number of unlike interactions are both optimal.

## B. Polytetrahedral transitions in the 55-atom Ar–Xe clusters

The cubic to icosahedral transition seen above actually favors polyicosahedral (or anti-Mackay) structures. The strain reduction produced by size disparity in 38-atom Ar–Xe clusters helps in stabilizing these kinds of structures, which are otherwise replaced by multilayer (or Mackay) geometries in the homogeneous clusters. Since most LJ clusters under the size of 38 atoms are most stable as polytetrahedra,<sup>55</sup> we do not expect that changing composition will affect them to a large extent. As a notable exception, the 6-atom homogeneous LJ cluster is more stable in its octahedral isomer. The lowest energy geometries of mixed Ar–Xe clusters containing 6 atoms, represented in Fig. 5, show polytetrahedral transitions for two compositions, namely Ar<sub>4</sub>Xe<sub>2</sub> and Ar<sub>3</sub>Xe<sub>3</sub>. This behavior mimics somewhat what was observed for the larger 38-atom cluster, only at a smaller scale. In particular, and as in Fig. 2, polytetrahedral arrangements are seen to be more convenient for Xenon compositions under 50%.

Possible polytetrahedral structures of mixed Ar–Xe clusters have been investigated for the size 55, whose most stable isomer is well known as a perfect double layer (Mackay) icosahedron for the homogeneous system. The global optimization results are summarized in Table IV for all compositions. For this we also conducted complementary calculations on the 2-layer lattice. Each putative global minimum was labelled either as Mackay icosahedron or, when the lattice structure does not exactly match the multilayer icosahedron, as polytetrahedral. Most compositions become increasingly polytetrahedral as the ratio of Xenon atoms increases, even though the polytetrahedral character may often be only local.

Two examples of lowest energy structures are represented in Fig. 6, corresponding to  $n = 15$  and  $n = 40$ . The obvious deviations of the geometry of the former from the Mackay icosahedron and the various occupation sites of the heavy atoms for both structures illustrate again that there is no simple rule that determine the most stable minima when the atomic sizes do significantly differ from each other.

## C. Temperature-induced transitions

We now go back to the 38-atom clusters of Kr and Xe atoms, for which the global minimum was always found to be a truncated octahedron. The extremely large number of isomers (including homotops) in the energy landscape of binary Lennard-Jones clusters, added to the expected presence of significant energy barriers between icosahedral and cubic isomers,<sup>40</sup> prevent finite-temperature simulations from being conducted in a reliably ergodic way with the presently available tools. For example, the particle exchange moves used to accelerate convergence of sampling among homotops will likely have very low ac-

ceptance probabilities in MC simulations at low temperatures, especially for Ar–Xe clusters. Therefore, even with powerful methods such as parallel tempering or multi-canonical Monte Carlo, reaching convergence in 38-atom LJ clusters does not seem currently feasible to us.

As an alternative, we have chosen to investigate solid-solid transitions by means of the superposition approach.<sup>59,60</sup> For a given cluster, databases of minima in each of the icosahedral (ICO) and truncated octahedral (FCC) funnels were constructed using the optimization algorithm. For each composition and each of the two funnels, no more than 2000 distinct minima were considered. The classical partition function of the Y<sub>38-p</sub>Xe<sub>p</sub> cluster (Y=Ar or Kr) restricted to funnel A=FCC or ICO is approximated by a harmonic superposition over all minima of the databases, which belong to this funnel:<sup>60</sup>

$$Q_A(\beta) = \sum_{i \in A} n_i \frac{\exp(-\beta E_i)}{(\beta h \bar{\nu}_i)^{3n-6}}, \quad (2)$$

where  $\beta = 1/k_B T$  is the inverse temperature,  $\bar{\nu}_i$  the geometric mean vibrational frequency,  $n_i = 2p!(n-p)!/h_i$  with  $h_i$  the order of the point group of minimum  $i$  and  $n = 38$ . We do not consider quantum effects here, although they may be important at low temperatures,<sup>61</sup> since delocalization or zero-point effects are not expected to be significant for rare gases as heavy as krypton or xenon.

Within the harmonic superposition approximation, a solid-solid transition occurs when  $Q_{\text{FCC}} = Q_{\text{ICO}}$ .<sup>62</sup> This latter equation is solved numerically in  $\beta$  or  $T$ , its solution is denoted  $T_{\text{ss}}$ . In cases where icosahedra are energetically more stable than octahedra, a solid-solid transition can occur if some cubic structures are entropically favored, which requires lower vibrational frequencies and/or lower symmetries. We did not find such situations in our samples of Ar–Xe clusters, therefore we restrict to Kr–Xe clusters in the following.

Similar to transitions between funnels, transitions between homotops will happen if their partition functions are equal. The huge number of homotops gives rise to as many values for the corresponding temperatures, and we define the homotop transition temperature  $T_h$  such that

$$T_h = \min_j \{T_h^{(j)} \mid T_h^{(j)} > 0\}, \quad (3)$$

where  $T_h^{(j)}$  is the transition temperature between the global minimum (homotop 0) and its homotop  $j$ .

Equating the harmonic partition functions for these two isomers leads to the expression of  $T_h^{(j)}$ .<sup>62</sup>

$$k_B T_h^{(j)} = \frac{E_j - E_0}{(3n-6) \ln \bar{\nu}_0 / \bar{\nu}_j + \ln n_j / n_0}. \quad (4)$$

Since all homotops are characterized by different vibrational and symmetry properties, the transition temperatures  $T_h^{(j)}$  are not ordered exactly as the energy differences  $E_j - E_0$ . This reflects that solid-solid transitions involve crossover in free energy rather than binding energy.



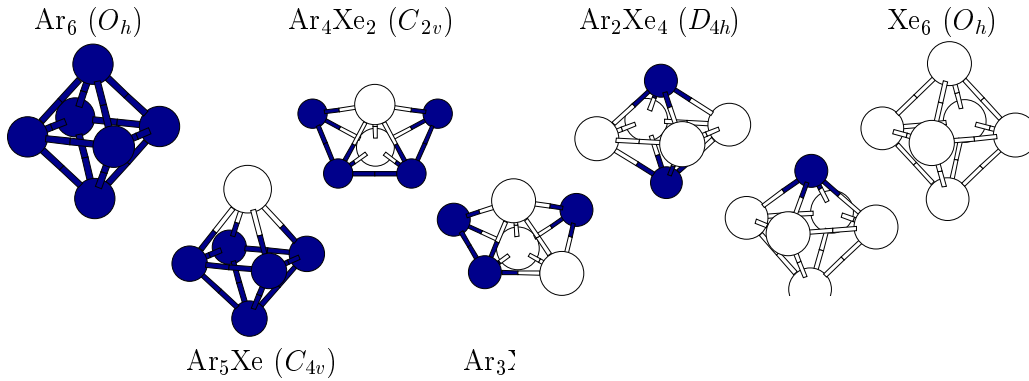
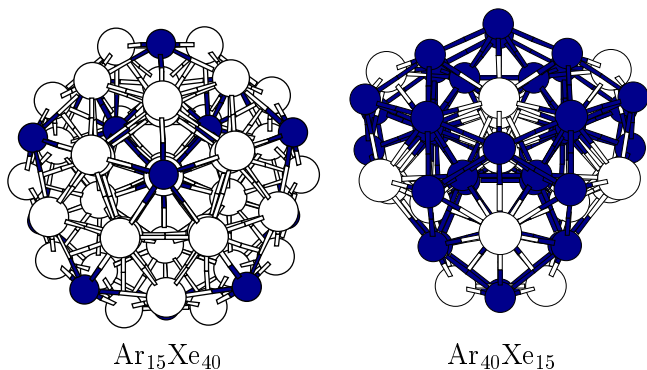


FIG. 5: Lowest energy stru

FIG. 6: Lowest energy structures of the  $\text{Ar}_{15}\text{Xe}_{40}$  and  $\text{Ar}_{40}\text{Xe}_{15}$  clusters. Both structures have  $C_{2v}$  symmetry.

The above equation also shows that  $T_h^{(j)}$  can take negative values if homotop  $j$  has a higher symmetry and/or a higher vibrational frequency than the ground state. In this case the global minimum is always the free energy minimum, and no solid-solid transition occurs, hence the form of Eq. (3).

Finally, a third temperature has a strong consequence on cluster structure, namely the melting temperature. Its estimation from either simulations or superpositions approximations is already quite difficult for the homogeneous  $\text{LJ}_{38}$  cluster,<sup>40,41</sup> and we did not attempt to compute it for binary clusters. However, the previous study by Frantz<sup>18</sup> has shown that the melting point in mixed, 13-atom Ar–Kr clusters varies quite regularly (approximately quadratically) with composition. As a simple rule, we will assume that the melting point of  $\text{Kr}_{38-n}\text{Xe}_n$ ,  $T_{\text{melt}}(n)$ , lies inside some range between the approximate melting points of  $\text{Kr}_{38}$  and  $\text{Xe}_{38}$ , respectively. From the results obtained by Doye and Wales<sup>40</sup> and the Monte Carlo data of Ref. 41 for the  $\text{LJ}_{38}$  cluster, we get  $T_{\text{melt}}(0) \simeq 0.234$  and  $T_{\text{melt}}(38) \simeq 0.315$  in reduced LJ units of argon. This provides rough limits to the actual melting points of Kr–Xe clusters, for the price of neglecting finite-size effects.

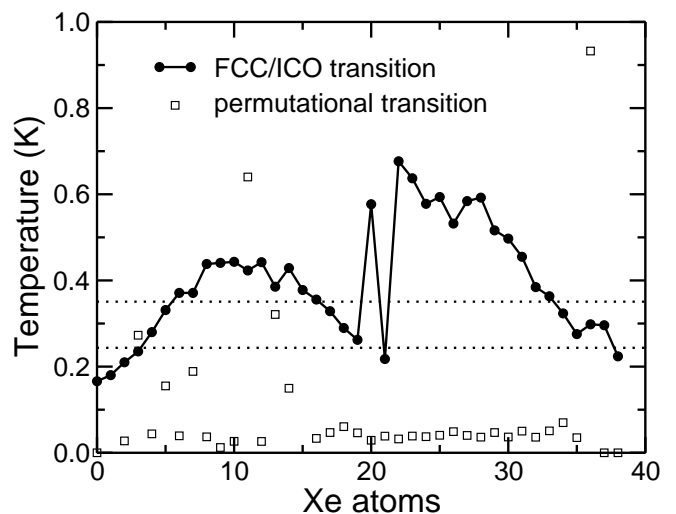


FIG. 7: Solid-solid transition temperature (full circles) between the octahedral and icosahedral funnels, estimated from a harmonic superposition approximation, versus composition in  $\text{Kr}_{38-n}\text{Xe}_n$  clusters. Also shown is the lowest transition temperature for a permutation between octahedral homotops. The horizontal dotted lines mark upper and lower limits for the estimated melting points. The temperatures are given in LJ units for argon (120 K).

The transition temperatures are represented in Fig. 7 for all compositions in  $\text{Kr}_{38-n}\text{Xe}_n$  clusters. We notice first that the structural transition temperature  $T_{\text{ss}}$  varies quite regularly with composition in both the ranges  $n < 19$  and  $n > 21$ , and that it shows strong size effects between these limits. Several situations are predicted to occur depending on the relative values of  $T_{\text{ss}}$ ,  $T_h$  and  $T_{\text{melt}}$ .

In most cases,  $T_{\text{melt}} < T_{\text{ss}}$ . That melting takes place at temperatures lower than the cubic/icosahedral transition simply nullifies the transition between structural types. However, this extra stability of the octahedral funnel may have a consequence on the melting point itself, which is likely to increase. Still, this situation implies that simu-

TABLE IV: Global optimization results for  $\text{Ar}_{55-n}\text{Xe}_n$ . The energies are given in LJ units for argon, and the symmetry and mixing ratios defined by Eq. (1) are reported. The structural types (Mackay Icosahedron MI or polytetrahedral PT) are also given.

$n$	Mixing ratio	Energy	Point group	Type	$n$	Mixing ratio	Energy	Point group	Type
0	0	-279.248	$I_h$	MI	28	0.53	-417.785	$C_1$	PT
1	0.05	-284.276	$C_{2v}$	MI	29	0.53	-421.225	$C_s$	PT
2	0.10	-289.313	$C_s$	MI	30	0.51	-424.566	$C_1$	PT
3	0.15	-294.360	$C_s$	MI	31	0.49	-427.888	$C_1$	PT
4	0.28	-302.344	$C_s$	PT	32	0.47	-431.565	$C_1$	PT
5	0.34	-310.780	$C_s$	PT	33	0.46	-435.680	$C_1$	PT
6	0.38	-316.331	$C_s$	PT	34	0.45	-439.565	$C_1$	PT
7	0.41	-321.770	$C_1$	PT	35	0.42	-443.335	$C_1$	PT
8	0.43	-327.241	$C_s$	PT	36	0.41	-446.892	$C_1$	PT
9	0.44	-332.356	$C_1$	PT	37	0.41	-449.965	$C_1$	PT
10	0.47	-337.497	$C_s$	PT	38	0.36	-454.356	$C_s$	MI
11	0.50	-342.655	$C_s$	PT	39	0.35	-458.203	$C_s$	MI
12	0.55	-347.608	$C_1$	PT	40	0.34	-462.564	$C_{2v}$	MI
13	0.57	-352.520	$C_1$	PT	41	0.30	-466.709	$C_{2v}$	MI
14	0.56	-357.586	$C_s$	PT	42	0.28	-472.191	$I_h$	MI
15	0.58	-362.483	$C_{2v}$	PT	43	0.26	-475.967	$C_{5v}$	MI
16	0.58	-367.231	$C_1$	PT	44	0.24	-479.739	$D_{5d}$	MI
17	0.59	-372.016	$C_s$	PT	45	0.22	-483.495	$C_{3v}$	MI
18	0.59	-376.740	$C_1$	PT	46	0.20	-487.219	$C_{2v}$	MI
19	0.59	-381.501	$C_{2v}$	PT	47	0.18	-490.910	$C_s$	MI
20	0.60	-386.007	$C_s$	PT	48	0.16	-494.585	$C_2$	MI
21	0.60	-390.135	$C_1$	PT	49	0.14	-498.231	$C_s$	MI
22	0.59	-395.065	$C_1$	PT	50	0.12	-501.860	$C_{2v}$	MI
23	0.59	-399.213	$C_1$	PT	51	0.10	-505.467	$C_{3v}$	MI
24	0.60	-403.205	$C_1$	PT	52	0.08	-509.052	$D_{5d}$	MI
25	0.58	-406.983	$C_1$	PT	53	0.06	-512.616	$C_{5v}$	MI
26	0.56	-410.686	$C_1$	PT	54	0.04	-516.170	$I_h$	MI
27	0.56	-414.427	$C_s$	PT	55	0	-517.168	$I_h$	MI

lations will more easily reach convergence.

However, there are notable exceptions for this behavior, at  $n < 4$ ,  $n = 21$  and  $n > 34$ . In these clusters, heterogeneity is not sufficient for the thermodynamical behavior of the cluster to deviate too much from those of the homogeneous system.

The transition between homotops usually occurs prior to melting. Thermal equilibrium within the cubic funnels thus involves several homotops (and “restricted” solid-solid transitions), and the corresponding thermodynamical state could be probably simulated using specifically designed exchange moves between outer particles within a Monte Carlo scheme.

A few clusters melt before exhibiting any transition between homotops. This occurs for instance at  $n = 11$ , 13 or 15. For these sizes the structural transition also occurs at temperatures higher than the estimated melting point. These cases should pose less problems to conventional simulations than the homogeneous cluster.

#### D. Glassy behavior

The previous results have shown that finite-size Ar–Xe compounds show a preferential polytetrahedral order, even for very low doping rates, over octahedral order. On the other hand, Kr–Xe clusters at the same sizes further favor cubic order. Since polytetrahedral order is known to be present in liquids and, more generally, in disordered structural glasses, it seems natural to correlate the behavior observed in these clusters to the dynamics of the corresponding bulk materials.<sup>29</sup>

We have simulated the cooling of 108-atom binary rare-gas liquids, using a simple Metropolis Monte Carlo scheme under constant volume and temperature. Initially the atoms are placed randomly into a cubic box of side  $L$ , and periodic boundaries are treated in the minimum image convention. The LJ interactions were not truncated, and the simulations consisted of 100 stages of  $10^5$  MC cycles each, linearly spaced in temperature.

Three compositions have been selected, following our

knowledge of the cluster structure. For each composition, different length sizes  $L$  and different temperature ranges  $[T_{\min}, T_{\max}]$  were chosen in order to cover both sides of the melting point. In the first mixture, 24 xenon atoms and 84 argon atoms are simulated with  $L = 4.8815$  LJ units of argon, with  $0.1 \leq T \leq 1$ . In the second mixture, 24 xenon atoms are added to 84 krypton atoms at  $L = 5.487$  and  $0.15 \leq T \leq 1.5$ . The third mixture consists of 9 argon atoms and 99 xenon atoms at  $L = 5.887$  and  $0.2 \leq T \leq 2$ . Even though we did not attempt to locate the most stable crystalline forms for these mixtures, our searches close to the face-centred cubic morphology showed that the most stable configurations for these mixtures always had some cubic order. It is likely that the actual ground states for such systems are indeed crystalline.<sup>63</sup>

The average root mean square fluctuation of the bond distances, also known as the Lindemann index  $\delta$ , universally characterizes the thermodynamical state of the condensed system as either solid or liquid, depending on its value being lower or higher than about 0.15. To quantify the extent of crystalline order, we have used the bond order parameter  $Q_4$  introduced by Steinhardt and coworkers.<sup>64</sup> The two parameters  $\delta$  and  $Q_4$  allow us to follow in Monte Carlo time the cooling processes for all materials in a simultaneous way, independently of thermodynamical characteristics such as the melting temperature.

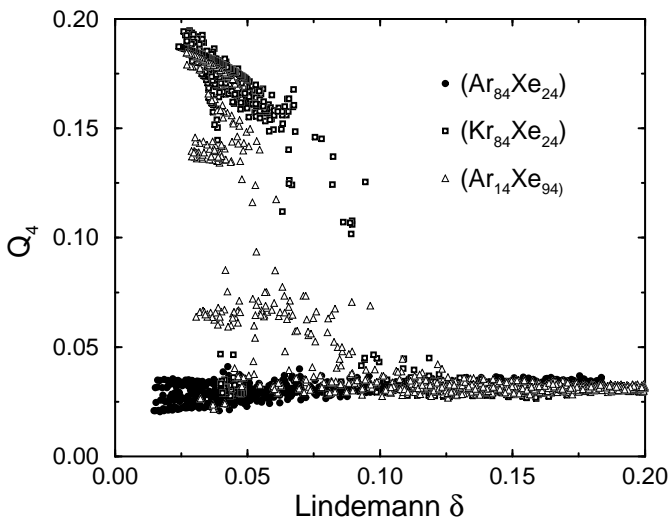


FIG. 8: Correlation between the Lindemann parameter  $\delta$  and the order parameter  $Q_4$  along cooling simulations of Ar–Xe and Kr–Xe bulk mixtures.

The correlation between  $\delta$  and  $Q_4$  for ten cooling simulations of each of the three bulk binary compounds is represented in Fig. 8. In all cases, the Lindemann parameter covers the whole range  $0.01 < \delta < 0.18$ , indicating that the melting point was indeed crossed. However, the three compounds display very contrasted cooling behaviors.

In the  $(\text{Ar}_{84}\text{Xe}_{24})$  system,  $\delta$  regularly decreases but  $Q_4$  always remain below 0.05. Therefore crystallization never takes place, and the final state obtained by quenching is significantly higher in energy than some crystalline forms; this is typical of glass formation.

In  $(\text{Kr}_{84}\text{Xe}_{24})$ , all simulations show some rather sharp transition from a (high  $\delta$ , low  $Q_4$ ) state to a (low  $\delta$ , high  $Q_4$ ) state as  $\delta$  crosses about 0.1. The temperatures where crystallisation occurs may vary somewhat among the cooling runs, in the same way as they are expected to depend on the cooling rate. Lastly, the case of  $(\text{Ar}_9\text{Xe}_{99})$  is intermediate: while most simulations end up in a nearly fully crystalline phase ( $Q_4 \sim 0.15$ ), a few of them show a limited degree of cubic ordering in the solid phase,  $Q_4$  having values close to 0.07.

These results very closely reflect our previous data on binary, 38-atom clusters of the same materials. In terms of composition, the first mixture corresponds to  $\text{Ar}_{30}\text{Xe}_8$ , which clearly favors icosahedral shapes over truncated octahedra. The second mixture reminds of  $\text{Kr}_{30}\text{Xe}_8$ , for which the cubic structure is even more stable than in the homogeneous cluster. The third mixture should be compared to  $\text{Ar}_3\text{Xe}_{35}$ , which favors icosahedra only moderately.

This correlation found here between cluster structure and the glassforming ability of the bulk material confirms previous analyses on the icosahedral local order in liquids and glasses,<sup>29,38</sup> as well as the recent conclusions obtained by Doye *et al.*<sup>39</sup> that clusters of good glassformers indeed show a polytetrahedral order.

#### IV. CONCLUSION

As far as structural and dynamical properties are concerned, binary compounds show a significantly richer complexity with respect to homogeneous clusters. The work reported in the present paper was intended to achieve several goals. First, a parallel global optimization algorithm was designed to locate the most stable structures of mixed rare-gas clusters, beyond the lattice approximations of Robertson and co-workers.<sup>51</sup> Based on the basin-hopping or Monte Carlo+minimization algorithm,<sup>44,45</sup> this algorithm includes exchange moves between particles at fixed composition as well as exchange moves between configurations at different compositions. Tests on simple  $\text{Ar}_n\text{Xe}_{13-n}$  and  $\text{Ar}_n\text{Xe}_{19-n}$  clusters show that the method is quite efficient, in addition to being easy to implement. For these systems, we have found that the choice of a very low temperature works best as it allows some significant time to be spent for optimizing the search for homotops on a same common lattice.

Putative global minima for  $\text{Ar}_{38-n}\text{Xe}_n$  and  $\text{Kr}_{38-n}\text{Xe}_n$  clusters have been investigated for all compositions. The structure of Ar–Xe compounds is mainly polytetrahedral, except at very low doping rates. Kr–Xe clusters not only remain as truncated octahedra, but mixing the two rare

gases even favors these cubic structures over icosahedra. We see some significant trend toward core/surface phase separation in Ar–Xe clusters with  $n > 20$  and in all Kr–Xe clusters. However, these demixing behaviors are not due to the same factors, as Xe atoms favor outer sites to reduce strain in Ar–Xe icosahedra, while they occupy interior sites to maximize the number of bonds in Kr–Xe truncated octahedra. Conversely,  $\text{Ar}_{38-n}\text{Xe}_n$  clusters with  $n < 20$  exhibit a higher degree of mixing. Analysing the strain in these stable structures confirms the presence of a structural transition near  $n = 20$  in these systems.

Polytetrahedral morphologies were also found as the most stable structures of many mixed Ar–Xe clusters with 55 atoms, as soon as the relative number of Xe atoms was large enough. The general conclusion thus seems that the extra strain introduced by mixing these different elements penalizes the highly ordered (cubic or 2-layer icosahedron) structures.

Within the harmonic superposition approximation, we have estimated the temperatures required by the 38-atom Kr–Xe clusters to undergo a structural transition toward the icosahedral funnel, or toward other octahedral homotops. For compositions with a doping rate higher than  $3/38$ , the structural transition temperature was seen to occur at temperatures higher than the extrapolated melting point. This mainly reflects the special stability of the octahedral structures, and has the probable consequence that actual melting points increase somewhat. These predictions could probably be checked with numerical simulations. For most compositions, the transitions between

different homotops of the truncated octahedron are seen to be potentially induced by relatively small temperatures. Therefore particle exchange moves will be necessary in order that simulations remain close to ergodic.

Following previous results by other researchers,<sup>29,38,39</sup> we have found some further evidence that criteria for glass formation in bulk materials may also lie in the parameters, which are responsible for stable cluster structures. Since the atomistic simulation of the dynamical vitrification process can generally be much harder than obtaining stable configurations of atomic clusters, we expect the approach followed in the present theoretical effort to be also useful in the community of glasses and supercooled liquids.

The method is obviously not limited to rare-gases, and its application to other compounds, especially metallic nanoalloys, should be straightforward, except maybe for fine tuning its intrinsic parameters. From a methodological point of view, it could also be applied to materials with more than two components. Work on ternary systems is currently in progress.

## V. ACKNOWLEDGMENTS

We wish to thank Dr. J. P. K. Doye and Prof. K. J. Jordan for very useful discussions. This research was supported by the CNRS-TUBITAK grant number 15071.

- 
- <sup>1</sup> S. Chacko, M. Deshpande, and D. G. Kanhere, *Phys. Rev. B* **64**, 155409 (2001).
- <sup>2</sup> S. Bromley, G. Sankar, C. R. A. Catlow, T. Maschmeyer, B. F. G. Johnson, and J. M. Thomas, *Chem. Phys. Lett.* **340**, 524 (2001).
- <sup>3</sup> B. K. Rao, S. Ramos de Debiaggi, and P. Jena, *Phys. Rev. B* **64**, 024418 (2001).
- <sup>4</sup> J. Jellinek and E. B. Krissinel, *Chem. Phys. Lett.* **258**, 283 (1996); E. B. Krissinel and J. Jellinek, *ibid.* **272**, 301 (1997).
- <sup>5</sup> J. L. Rousset, A. M. Cadrot, F. J. Cadete Santos Aires, A. Renouprez, P. Mélinon, A. Perez, M. Pellarin, J. L. Vialle, and M. Broyer, *J. Chem. Phys.* **102**, 8574 (1995).
- <sup>6</sup> M. J. López, P. A. Marcos, and J. A. Alonso, *J. Chem. Phys.* **104**, 1056 (1996).
- <sup>7</sup> G. E. López and D. L. Freeman, *J. Chem. Phys.* **98**, 1428 (1993).
- <sup>8</sup> I. L. Garzon, X. P. Long, R. Kawai, and J. H. Weare, *Chem. Phys. Lett.* **158**, 525 (1989).
- <sup>9</sup> P. Ballone, W. Andreoni, R. Car, and M. Parrinello, *Europhys. Lett.* **8**, 73 (1989).
- <sup>10</sup> S. Darby, T. V. Mortimer-Jones, R. L. Johnston, and C. Roberts, *J. Chem. Phys.* **116**, 1536 (2002).
- <sup>11</sup> M. S. Bailey, N. T. Wilson, C. Roberts, and R. L. Johnston, *Euro. Phys. J. D* **25**, 41 (2003).
- <sup>12</sup> M. C. Vicéns and G. E. López, *Phys. Rev. A* **62**, 033203 (2000).
- <sup>13</sup> F. Baletto, C. Mottet, and R. Ferrando, *Phys. Rev. Lett.* **90**, 135504 (2003).
- <sup>14</sup> E. Fort, A. De Martino, F. Pradère, M. Châtelet, and H. Vach, *J. Chem. Phys.* **110**, 2579 (1999); H. Vach, *ibid.* **111**, 3536 (1999); **113**, 1097 (2000).
- <sup>15</sup> M. Tchapyguine, R. R. T. Marinho, M. Gisselbrecht, R. Feifel, S. L. Sorensen, G. Öhrwall, M. Lundwall, A. Naves de Brito, J. Schulz, N. Mårtensson, S. Svensson, and O. Björneholm, *J. Chem. Phys.* **120**, 345 (2004); M. Tchapyguine, M. Lundwall, M. Gisselbrecht, G. Öhrwall, R. Feifel, S. Sorensen, S. Svensson, N. Mårtensson, and O. Björneholm, *Phys. Rev. A* **69**, 031201 (2004).
- <sup>16</sup> F. G. Amar and J. Smaby (private communication).
- <sup>17</sup> J. P. K. Doye, M. A. Miller, and D. J. Wales, *J. Chem. Phys.* **111**, 8417 (1999).
- <sup>18</sup> D. D. Frantz, *J. Chem. Phys.* **105**, 10030 (1996).
- <sup>19</sup> D. D. Frantz, *J. Chem. Phys.* **107**, 1992 (1997).
- <sup>20</sup> G. S. Fanourgakis, P. Parneix, and Ph. Bréchnignac, *Euro. Phys. J. D* **24**, 207 (2003).
- <sup>21</sup> L. J. Munro, A. Tharrington, and K. J. Jordan, *Comp. Phys. Comm.* **145**, 1 (2002).
- <sup>22</sup> C. Chakravarty, *J. Chem. Phys.* **104**, 7223 (1996).
- <sup>23</sup> D. Sabo, J. D. Doll, and D. L. Freeman, *J. Chem. Phys.* **118**, 7321 (2003).
- <sup>24</sup> D. Sabo, J. D. Doll, and D. L. Freeman, *J. Chem. Phys.* **121**, 847 (2004).
- <sup>25</sup> D. Sabo, C. Predescu, J. D. Doll, and D. L. Freeman, *J.*

- Chem. Phys. **121**, 856 (2004).
- <sup>26</sup> P. Parneix, Ph. Bréchnignac, and F. Calvo, Chem. Phys. Lett. **381**, 471 (2003).
- <sup>27</sup> F. Calvo, J. P. K. Doye, and D. J. Wales, J. Chem. Phys. **116**, 2642 (2002).
- <sup>28</sup> A. S. Clarke, R. Kapral, B. Moore, G. Patey, and X.-G. Wu, Phys. Rev. Lett. **70**, 3283 (1993); A. S. Clarke, R. Kapral, and G. N. Patey, J. Chem. Phys. **101**, 2432 (1994).
- <sup>29</sup> H. Jónsson and H. C. Andersen, Phys. Rev. Lett. **60**, 2295 (1988).
- <sup>30</sup> W. Kob and H. C. Andersen, Phys. Rev. E **51**, 4626 (1995).
- <sup>31</sup> B. Coluzzi, G. Parisi, and P. Verocchio, J. Chem. Phys. **112**, 2933 (2000).
- <sup>32</sup> M. Utz, P. G. Debenedetti, F. H. Stillinger, Phys. Rev. Lett. **84**, 1471 (2000).
- <sup>33</sup> K. K. Bhattacharya, K. Broderix, R. Kree, and A. Zippelius, Europhys. Lett. **47**, 449 (1999).
- <sup>34</sup> R. Yamamoto and W. Kob, Phys. Rev. E **61**, 5473 (2000).
- <sup>35</sup> H.-J. Lee, T. Cagin, W. L. Johnson, and W. A. Goddard, J. Chem. Phys. **119**, 9858 (2003).
- <sup>36</sup> F. C. Frank, Proc. R. Soc. London, Ser. A **215**, 43 (1952).
- <sup>37</sup> T. Schenk, D. Holland-Moritz, V. Simonet, R. Bellissent, and D. M. Herlach, Phys. Rev. Lett. **89**, 075507 (2002).
- <sup>38</sup> S. Mossa and G. Tarjus, J. Chem. Phys. **119**, 8069 (2003).
- <sup>39</sup> J. P. K. Doye, D. J. Wales, F. H. M. Zetterling, and M. Dzugutov, J. Chem. Phys. **118**, 2792 (2003).
- <sup>40</sup> J. P. K. Doye, M. A. Miller, and D. J. Wales, J. Chem. Phys. **110**, 6896 (1999).
- <sup>41</sup> J. P. Neirotti, F. Calvo, D. L. Freeman, and J. D. Doll, J. Chem. Phys. **112**, 10340 (2000).
- <sup>42</sup> D. J. Wales and H. A. Scheraga, Science **285**, 1368 (1999).
- <sup>43</sup> B. Hartke, Chem. Phys. Lett. **258**, 144 (1996).
- <sup>44</sup> Z. Li and H. A. Scheraga, Proc. Natl. Acad. Sci. USA **84**, 6611 (1987).
- <sup>45</sup> D. J. Wales and J. P. K. Doye, J. Phys. Chem. A **101**, 5111 (1997).
- <sup>46</sup> D. J. Wales, J. P. K. Doye, A. Dullweber, M. P. Hodges, F. Y. Naumkin, F. Calvo, J. Hernández-Rojas and T. F. Middleton, URL <http://www-wales.ch.cam.ac.uk/CCD.html>.
- <sup>47</sup> G. J. Geyer, in *Computing Science and Statistics: Proceedings of the 23rd Symposium on the Interface*, ed. by E. K. Keramidas (Interface Foundation, Fairfax Station, 1991), p. 156.
- <sup>48</sup> D. Gazzillo and G. Pastore, Chem. Phys. Lett. **159**, 388 (1989).
- <sup>49</sup> H. Karaaslan and E. Yurtsever, Chem. Phys. Lett. **187**, 8 (1991).
- <sup>50</sup> T. S. Grigera and G. Parisi, Phys. Rev. E **63**, 045102(R) (2001).
- <sup>51</sup> D. H. Robertson, F. B. Brown, and I. M. Navon, J. Chem. Phys. **90**, 3221 (1989).
- <sup>52</sup> D. M. Leitner, J. D. Doll, and R. M. Whitnell, J. Chem. Phys. **94**, 6644 (1991).
- <sup>53</sup> J. P. K. Doye, M. A. Miller, and D. J. Wales, J. Chem. Phys. **109**, 8143 (1998).
- <sup>54</sup> H. Karaaslan and E. Yurtsever, Ber. Bunsenges. Phys. Chem. **98**, 47 (1994).
- <sup>55</sup> J. A. Northby, J. Chem. Phys. **87**, 6166 (1987).
- <sup>56</sup> J. Pillardy and L. Piela, J. Phys. Chem. **99**, 11805 (1995).
- <sup>57</sup> J. P. K. Doye, D. J. Wales, and R. S. Berry, J. Chem. Phys. **103**, 4234 (1995).
- <sup>58</sup> F. Calvo, F. Spiegelman, and M.-C. Heitz, J. Chem. Phys. **118**, 8739 (2003).
- <sup>59</sup> F. H. Stillinger and T. A. Weber, Phys. Rev. A **25**, 978 (1982).
- <sup>60</sup> D. J. Wales, Mol. Phys. **78**, 151 (1993).
- <sup>61</sup> F. Calvo, J. P. K. Doye, and D. J. Wales, J. Chem. Phys. **114**, 7312 (2001).
- <sup>62</sup> J. P. K. Doye and F. Calvo, Phys. Rev. Lett. **86**, 3570 (2001).
- <sup>63</sup> T. F. Middleton, J. Hernández-Rojas, P. N. Mortenson, and D. J. Wales, Phys. Rev. B **64**, 184201 (2001); J. R. Fernández and P. Harrowell, Phys. Rev. E **67**, 011403 (2003); J. Chem. Phys. **120**, 9222 (2004).
- <sup>64</sup> P. J. Steinhardt, D. R. Nelson, and M. Ronchetti, Phys. Rev. B **28**, 784 (1983).

TABLE V: Global optimization results for  $\text{Kr}_{38-n}\text{Xe}_n$ . The energies are given in LJ units for argon, and the symmetry and mixing ratios defined by Eq. (1) are reported.

$n$	Mixing ratio	Energy	Point group	$n$	Mixing ratio	Energy	Point group
0	0	-238.897	$O_h$	20	0.45	-286.209	$C_s$
1	0.09	-241.200	$C_s$	21	0.44	-288.240	$C_s$
2	0.18	-243.604	$C_{2v}$	22	0.42	-290.323	$C_{2v}$
3	0.25	-245.962	$C_s$	23	0.42	-292.310	$C_s$
4	0.27	-248.453	$C_s$	24	0.41	-294.347	$O_h$
5	0.33	-250.927	$C_s$	25	0.37	-296.352	$C_{3v}$
6	0.35	-253.489	$C_{2v}$	26	0.35	-298.371	$C_{2v}$
7	0.39	-256.005	$C_s$	27	0.33	-300.382	$C_s$
8	0.41	-258.570	$D_{4h}$	28	0.32	-302.414	$C_{4v}$
9	0.43	-261.156	$C_s$	29	0.29	-304.411	$C_{4v}$
10	0.45	-263.740	$C_{2v}$	30	0.25	-306.457	$C_s$
11	0.47	-266.294	$C_s$	31	0.22	-308.390	$C_s$
12	0.48	-268.867	$C_s$	32	0.20	-310.370	$C_s$
13	0.49	-271.420	$C_s$	33	0.16	-312.315	$C_s$
14	0.50	-273.996	$C_{2v}$	34	0.13	-314.287	$C_{3v}$
15	0.50	-275.996	$C_s$	35	0.10	-316.230	$C_s$
16	0.50	-278.046	$D_{4h}$	36	0.07	-318.200	$D_{4h}$
17	0.48	-280.082	$C_s$	37	0.04	-320.133	$C_{4v}$
18	0.47	-282.129	$C_{2v}$	38	0	-322.115	$O_h$
19	0.46	-284.164	$C_s$				